Contents lists available at ScienceDirect

Experimental Eye Research

journal homepage: www.elsevier.com/locate/yexer

Involvement of increased endoplasmic reticulum stress in the development of cataracts in BALB.NCT-*Cpox*^{nct} mice

Chang Liu [a,b], Hiroki Miyahara [c], Jian Dai [c], Xiaoran Cui [a], Ying Li [a], Xiaojing Kang [a], Keiichi Higuchi [a,c], Masayuki Mori [a,c,*]

[a] Department of Aging Biology, Shinshu University Graduate School of Medicine, Science and Technology, 3-1-1 Asahi, Matsumoto 390-8621, Japan
[b] Department of Respiratory, The Third Hospital of Shijiazhuang, Shijiazhuang 050011, China
[c] Department of NeuroHealth Innovation, Institute for Biomedical Sciences, Interdisciplinary Cluster for Cutting Edge Research, Shinshu University, 3-1-1 Asahi, Matsumoto 390-8621, Japan

ARTICLE INFO

Keywords:
Cataract
Endoplasmic reticulum stress
Crystallin
Mouse
Coproporphyrin
Protein aggregation
Transcriptomics

ABSTRACT

The BALB.NCT-*Cpox*^{nct} is a mutant mouse model for hereditary cataracts. We previously uncovered that the primary cause of the cataracts of BALB.NCT-*Cpox*^{nct} is a mutation in the coproporphyrinogen oxidase (*Cpox*) gene. Because of the mutation, excessive coproporphyrin is accumulated in the BALB.NCT-*Cpox*^{nct} lens. In this study, we analyzed the changes in transcriptome and proteins in the lenses of 4- and 12-week-old BALB.NCT-*Cpox*^{nct} to further elucidate the molecular etiology of cataracts in this mouse strain. Transcriptome analysis revealed that endoplasmic reticulum (ER) stress was increased in the BALB.NCT-*Cpox*^{nct} lens that induced persistent activation of the PERK signaling pathway of the ER stress response. Also, levels of crystallin transcripts and proteins were reduced in the BALB.NCT-*Cpox*^{nct} lens. Analysis of proteins disclosed aggregation of crystallins and keratins prior to the manifestation of cataracts in 4-week-old BALB.NCT-*Cpox*^{nct} mice. At 12 weeks of age, insoluble crystallins were accumulated in the cataractous BALB.NCT-*Cpox*^{nct} lens. Overall, our data suggest the following sequence of events in the BALB.NCT-*Cpox*^{nct} lens: accumulated coproporphyrin induces the aggregation of proteins including crystallins. Aggregated proteins increase ER stress that, in turn, leads to the repression of global translation of proteins including crystallins. The decline in the molecular chaperone crystallin aggravates aggregation and insolubilization of proteins. This vicious cycle would eventually lead to cataracts in BALB.NCT-*Cpox*^{nct}.

1. Introduction

Nakano cataract (NCT) is a mouse model for hereditary cataracts and has been used to understand the mechanisms of cataractogenesis (Nakano et al., 1960; Takehana et al., 1990). The cataract of NCT is an autosomal recessive trait governed by a single locus, referred to as *nct*. NCT mice develop a pin-head opacity in the nucleus of the lens by the 24th postnatal day, followed by rapid opacification of the whole lens over the next 36 days. NCT mice also manifest retarded growth of the lens (Fukui et al., 1976). A previous study demonstrated that implantation of the normal lens from wild-type mice into the NCT eye resulted in normal growth and transparency of the implanted lens (Yamamoto and Iwata, 1973; Takehana, 1990). Conversely, implantation of the young NCT lens into the eye of wild-type mice resulted in the opaque lens by the 18th day after implantation. The results of this implantation study indicated that the development of cataracts in NCT mice is intrinsic to the lens. Meanwhile, a drawback of NCT was the absence of an authentic control because they have a different genetic background from commonly used mouse strains. To resolve this issue, a congenic strain in which the *nct* locus was introduced into the background of an inbred BALB/c strain (BALB.NCT-*nct*) was bred (Matsuzawa and Wada, 1988; Wada et al., 1991; Koyama-Ito and Wada, 1992). Unexpectedly but intriguingly, cataract phenotypes including the process of lens opacification and age at onset are altered in the BALB.NCT-*nct* congenic mice. Contrary to early onset and rapid progression of cataracts at around 4 weeks of age in NCT, none of BALB.NCT-*nct* congenic mice

* Corresponding author. Department of NeuroHealth Innovation, Institute for Biomedical Sciences, Interdisciplinary Cluster for Cutting Edge Research, Shinshu University, 3-1-1 Asahi, Matsumoto 390-8621, Japan.
E-mail addresses: 18hb307k@shinshu-u.ac.jp (C. Liu), 12mh207j@shinshu-u.ac.jp (H. Miyahara), daijian3@shinshu-u.ac.jp (J. Dai), 17mh282d@shinshu-u.ac.jp (X. Cui), 19hb307c@shinshu-u.ac.jp (Y. Li), 19hb304j@shinshu-u.ac.jp (X. Kang), keiichih@shinshu-u.ac.jp (K. Higuchi), masamori@shinshu-u.ac.jp (M. Mori).

https://doi.org/10.1016/j.exer.2021.108905
Received 12 October 2021; Received in revised form 26 November 2021; Accepted 20 December 2021

Table 1
Primers for real-time PCR.

Target RNA		Primer sequence
Atf4	Sense	CCTTCGACCAGTCGGGTTTG
	Antisense	CTGTCCCGGAAAAGGCATCC
Chop	Sense	TTGGAGACGGTGTCCAGCTG
	Antisense	ACGCAGGGTCAAGAGTAGTG
Bip	Sense	AACCCCGAGAACACGGTCTT
	Antisense	TGCCCACCTCCAATATCAACT
Calr	Sense	ACCAACCGCTGGGTCGAATC
	Antisense	GTCTGGCCCTTATTGCTGAAG
Cryaa	Sense	GCAAGTTACATGGCGAAGGTC
	Antisense	ATTGGAAGGCAGACGGTAGC
Cryab	Sense	CTGCAGGCAGGACATAGGTG
	Antisense	CCGCCAGTTCATGGAGACTT
Actb	Sense	ACAATGAGCTGCGTGTGGCC
	Antisense	CCTCGTAGATGGGCACAGTG

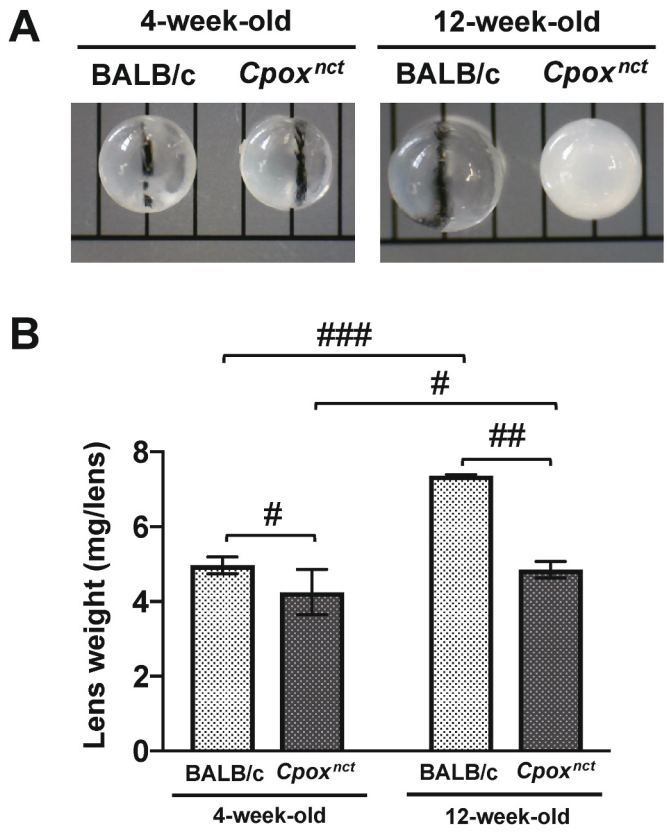

Fig. 1. Cataract and microphakia in BALB.NCT-*Cpox*^{nct}. (**A**) The appearance of lenses of BALB/c and BALB.NCT-*Cpox*^{nct} of 4- (left panel) and 12-week-old (right panel). Each unit of the scale represents 1 mm. (**B**) Comparison of lens weight between BALB/c and BALB.NCT-*Cpox*^{nct} at 4- and 12-week-old (mean ± SD; n = 3). Statistical differences were evaluated using the Student's *t*-test. $^{\#}P < 0.05$, $^{\#\#}P < 0.01$, $^{\#\#\#}P<0.001$.

develop cataracts by that age. Lens opacification in congenic mice commences in a diffuse, mild form at the cortex of the lens around 6 weeks of age and intensifies gradually. The median age of cataract incidence is approximately 8 weeks in females and 13 weeks in males. By 12 weeks of age, approximately 80% and 45% of the female and male congenic mice, respectively have cataracts. In addition, microphakia is milder in BALB.NCT-*nct* compared to NCT.

In a previous study, we uncovered that the *nct* locus is a hypomorphic missense mutation in the coproporphyrinogen oxidase gene (*Cpox*^{nct} mutant allele), encoding the enzyme responsible for catalyzing oxidative decarboxylation of the heme precursor, coproporphyrinogen III, in the heme biosynthetic pathway (Mori et al., 2013). Due to the mutation, CPOX activity in BALB.NCT-*Cpox*^{nct} was reduced to ~15% of that in wild-type BALB/c mice. Because of the reduction in CPOX activity, BALB.NCT-*Cpox*^{nct} mice had an exceedingly high level of coproporphyrin III, an autonomously oxidized form of coproporphyrinogen III in the serum and liver. Most importantly, coproporphyrin III was excessively accumulated also in the BALB.NCT-*Cpox*^{nct} lens: ~40 and ~60 nmol/g wet lens weight at 4 and 12 weeks of age, respectively, while only a trace amount was detected in the age-matched control BALB/c lens. In addition, transgenic expression of the wild-type CPOX in mice homozygous for the mutant *Cpox*^{nct} allele resulted in the reduction of coproporphyrin III level to the physiological level in the lens and prevention of cataracts. Overall, these results suggested that the cataracts of BALB.NCT-*Cpox*^{nct} mice stem from coproporphyrin III accumulation in the lens due to the *Cpox*^{nct} mutation. However, the etiological link of the coproporphyrin accumulation and cataracts remained unresolved.

Since our report of the identification of *Cpox*^{nct} as a cause of cataracts of BALB.NCT-*Cpox*^{nct}, several papers have been published. First, a series of papers reported the mechanisms of porphyrin intermediate to cause protein aggregation in cell culture models and more intriguingly in the liver of inducible mouse models of porphyria (Singla et al., 2013; Maitra et al., 2015, 2019b; Maitra et al., 2019a). These papers demonstrated that coproporphyrin binds proteins and leads, in the presence of oxygen, to protein oxidation and aggregation. Thus, accumulated coproporphyrin may give rise to the formation of protein aggregates and lens opacity in BALB.NCT-*Cpox*^{nct} as well. Second, transcriptome analysis has been demonstrated to be effective in improving our understanding of the molecular etiology of disease including cataracts (Hegde et al., 2014; Bennett et al., 2016; Andley et al., 2018; Ishida et al., 2020; Jia et al., 2021; Wang et al., 2021). Inspired by these reports, we analyzed the changes in transcriptome and proteins in this study to further elucidate the molecular etiology of cataracts in BALB.NCT-*Cpox*^{nct}.

2. Material and methods

2.1. Animals

Breeding pairs of inbred BALB.NCT-*Cpox*^{nct} congenic mice (RBRC00422) were obtained from the RIKEN BRC (Tsukuba, Japan) via the National BioResource Project of MEXT/AMED (Tokyo, Japan) and subsequently bred by brother × sister mating at the Institute of Experimental Animals, Shinshu University. The BALB/c mice were purchased from Japan SLC, Inc. (Hamamatsu, Japan) and used as controls. These mice were maintained under clean conventional conditions at 24 ± 2 °C with a light-controlled regimen (12 h light/dark cycle) and had free access to a commercial diet (MF; Oriental Yeast Co. Ltd., Tokyo, Japan) and tap water. All experimental procedures involving mice were conducted in accordance with the Regulations for Animal Experimentation of Shinshu University. The animal protocol was approved by the Committee for Animal Experiments of Shinshu University (approval number 300021).

2.2. RNA-seq analysis

Lenses were obtained from 4-week-old BALB/c mice (n = 5), 4-week-old BALB.NCT-*Cpox*^{nct} mice (n = 5), 12-week-old BALB/c mice (n = 3), and 12-week-old BALB.NCT-*Cpox*^{nct} mice (n = 3). After mice were sacrificed by cervical dislocation under deep anesthesia with isoflurane inhalation, the eyeballs were removed. The lenses were then dissected from the eyeball and weighed. The right and left lenses of a mouse were homogenized together in 1 mL of TRIZOL Reagent (Thermo Fisher Scientific, Waltham, MA, USA). Aliquots of the homogenate (0.333 mL for 4-week-old mice and 0.2 mL for 12-week-old mice) were pooled to make 1 mL homogenate. Total RNAs were extracted from the homogenates by

Table 2
List of 42 DEGs between the 4-week-old BALB/c and BALB.NCT-*Cpox*^{nct} lenses.

Upregulated gene	BALB/c read count[a]	BALB.NCT-*Cpox*^{nct} read count[a]	Log2 fold change	*q*-value	Downregulated gene	BALB/c read count[a]	BALB.NCT-*Cpox*^{nct} read count[a]	Log2 fold change	*q*-value
Chac1	0.00	19.89	6.05	0.00011949	*Avp*	126.84	1.19	−6.73	1.11E-24
Chop[b]	5.71	59.97	3.39	2.49E-13	*Serpina3h*[b]	57.05	7.49	−2.93	6.29E-06
Idi1[b]	23.60	121.55	2.36	4.01E-21	*Hspb1*[b]	1664.08	259.04	−2.68	4.52E-174
Hmgcs1[b]	58.08	273.40	2.24	2.75E-46	*Itgb1bp1*[b]	119.93	24.14	−2.31	4.15E-09
Scd1	16.70	61.35	1.88	3.76E-08	*Snx22*[b]	84.50	18.37	−2.20	1.21E-05
Hmgcr[b]	17.96	63.59	1.82	3.32E-08	*Hmox1*[b]	284.37	66.83	−2.09	6.59E-19
Fdft1	44.08	154.71	1.81	5.62E-21	*Tcp11*[b]	680.15	189.87	−1.84	2.35E-36
Msmo1	10.33	36.11	1.81	0.00023973	*Eif5b*[b]	522.08	171.31	−1.61	1.04E-20
Cyp51	26.79	85.20	1.67	3.05E-10	*Svbp*[b]	322.15	115.16	−1.48	2.96E-10
Nsdhl	10.99	34.49	1.65	0.00089687	*Pgam2*[b]	561.30	205.37	−1.45	1.68E-17
Arl2bp[b]	23.18	63.69	1.46	2.17E-06	*R3hdml*[b]	173.51	66.79	−1.38	0.00027208
Chrng[b]	28.65	78.47	1.45	4.72E-08	*Lgsn*[b]	5343.98	2123.97	−1.33	3.84E-142
Lss	32.19	84.96	1.40	2.15E-08	*Dapl1*[b]	310.08	133.00	−1.22	8.95E-06
Sqle[b]	23.12	59.49	1.36	1.67E-05	*Crygc*[b]	62195.56	26679.52	−1.22	3.43E-08
Insig1	113.69	289.43	1.35	2.41E-29	*Csrp1*[b]	235.31	103.38	−1.19	0.0006107
Sag[b]	25.46	59.06	1.21	9.02E-05	*Crygn*	685.26	326.25	−1.07	3.58E-09
Glo1	79.64	177.37	1.16	6.85E-15	*Cst3*[b]	344.97	168.59	−1.03	0.00074513
Atf4[b]	46.24	102.33	1.15	3.48E-08					
Olfm1	20.48	44.37	1.12	0.0035406					
Rbp3[b]	22.28	48.33	1.12	0.0016715					
Prph2[b]	23.06	49.95	1.11	0.0012714					
mt-Co1	1291.06	2783.73	1.11	1.88E-237					
Rho[b]	104.14	221.02	1.09	1.62E-17					
Otud1	24.08	50.04	1.06	0.0021056					
Gnat1[b]	38.68	79.86	1.05	1.37E-05					

[a] Count of reads obtained by RNA-seq analysis with an Illumina next-generation sequencing platform and adjusted by the edgeR package through one scaling normalized factor.
[b] Read counts for these 28 genes are statistically different between mouse strains also at 12 weeks of age.

using RNeasy Mini Kit (QIAGEN, Hilden, Germany).

RNA quality check, library preparation, RNA-seq analysis, and bioinformatics analysis of the data were conducted by Filgen Inc. (Nagoya, Japan). After isolation of poly-adenylated RNA using oligo(dT) beads, cDNA libraries were prepared using a NEBNext Ultra RNA Library Prep Kit for Illumina (New England BioLabs, Ipswich, USA). Paired-end reads (125 bp/150 bp) were generated using Illumina NovaSeq6000/PE150 next-generation sequencing platform (Illumina Inc., San Diego, USA). Raw RNA-seq reads were processed through in-house perl scripts to remove reads of low quality. The removed reads included those with adaptor contamination, with uncertain nucleotides constituting more than 10 percent of either read (N > 10%), and with low-quality nucleotides (base quality less than 20) constituting more than 50 percent of the read. TopHat v2.0.12 (Kim et al., 2013) was used to align paired-end read sequences to the UCSC *Mus musculus* full genome build (mm10) to generate bam files. The mismatch parameter was set to two, and other parameters were set to default. HTSeq v0.6.1 software (Anders et al., 2015) was used to analyze the gene expression levels using the union mode. The expected number of fragments per kilobase of transcript sequence per million base pairs sequenced (FPKM) was calculated based on the length of the gene and read count mapped to this gene (Trapnell et al., 2010). Prior to differential gene expression analysis, for each sequenced library, the read counts were adjusted by edgeR program package through one scaling normalized factor. Differential gene expression analysis between BALB/c and BALB.NCT-*Cpox*^{nct} at 4 and 12 weeks of age was then carried out by DEGseq R package 1.20.0 (Wang et al., 2010). The *P* values were adjusted using the Benjamini & Hochberg method (Benjamini and Hochberg, 1995). Corrected *P*-value of 0.005 and $\log_2$(fold change) of 1 were set as the threshold for significantly different expressions. The gene ontology (GO) enrichment analysis of differentially expressed genes was conducted using GOseq R package (Young et al., 2010), in which gene length bias was corrected. GO terms with a corrected *P* value less than 0.05 were considered significantly enriched.

2.3. Real-time reverse transcription PCR

Total RNA was extracted from the lens of mice using the TRIZOL Reagent. First-strand complementary DNA (cDNA) was synthesized from 1 μg of RNA using ReverTra Ace -α- reverse transcriptase (TOYOBO, Osaka, Japan). Quantitative real-time PCR was conducted using a sequence detection system (ABI PRISM 7500, Applied Biosystems, CA, USA) with SYBR Green Premix EX Taq™ II (TaKaRa Bio, Kusatsu, Japan). Each sample was run in triplicate for each primer set in any one of three independent experiments. The transcript for the housekeeping gene, beta-actin (*Actb*), was used to normalize the relative levels of transcripts between the different genotypes. The forward and reverse primer sequences are listed in Table 1.

2.4. Immunoblot analysis

Lenses were homogenized in ice-cold RIPA lysis buffer (Santa Cruz Biotechnology, Dallas, USA). The soluble fraction was separated by centrifugation (4 °C, 12,000 rpm, 15 min). The protein concentration in the soluble fraction was measured using a BCA Protein Assay Kit (Thermo Fisher Scientific). An aliquot equivalent to 20–50 μg protein was applied to SDS-PAGE (10–15%) and transferred to a polyvinylidene difluoride (PVDF) membrane (Immobilon, 0.2 μm pore, Millipore Corp., MA, USA). The membrane was then serially reacted with a primary antibody and horseradish peroxidase-conjugated secondary antibody. The target proteins were detected by enhanced chemiluminescence. Densitometric analysis of the target proteins was performed using the NIH ImageJ software. The primary antibodies included anti-BiP (Santa Cruz, sc-1050, USA), anti-eIF2α (Cell Signaling Technology, #9722, USA), anti-P-eIF2α (Abcam, ab32157, UK), anti-ATF4 (Proteintech, 10835-1-AP, USA), anti-CHOP (Proteintech,15204-1-AP, USA), anti-αB-crystallin (GeneTex, GTX103053, USA), anti-βB1-crystallin (Santa Cruz, sc-48335, USA), and anti-β-actin (Santa Cruz, sc-47778, USA). The secondary antibodies were anti-rabbit IgG (Cell Signaling Technology, 7074s, USA), or anti-mouse IgG (Cell Signaling Technology, 7076s,

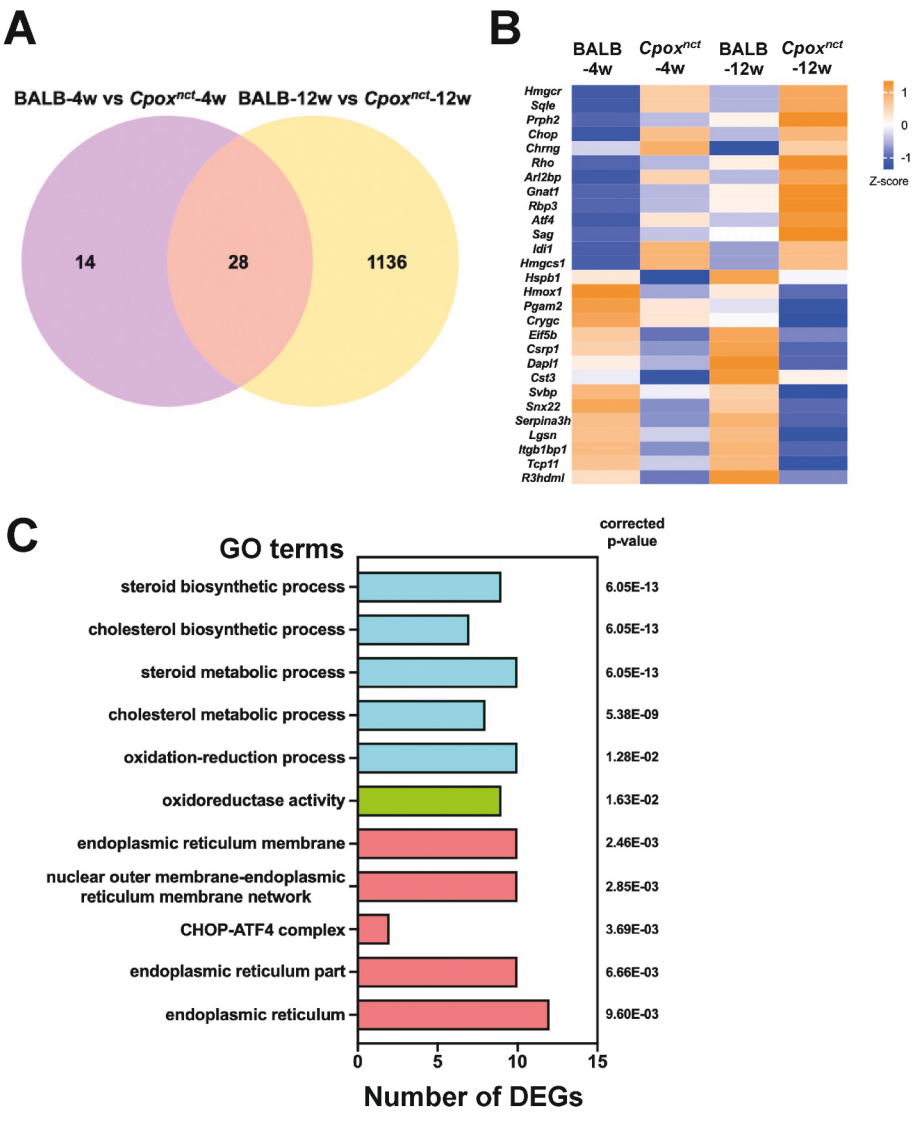

Fig. 2. Transcriptome analysis reveals a signature of increased endoplasmic reticulum stress in the BALB.NCT-*Cpox*^{nct} lens. (**A**) A Venn diagram showing the number of differentially expressed genes (DEGs) between BALB/c and BALB.NCT-*Cpox*^{nct} at 4- and 12-week-old, with the overlapping regions showing the number of common DEGs for the two time points. (**B**) Heat map of 28 common DEGs for the 4- and 12-week-old lenses. (**C**) A bar chart of the gene ontology terms (blue: biological process, green: molecular function, red: cellular component) for 42 DEGs between BALB/c and BALB.NCT-*Cpox*^{nct} at 4-week-old.

USA).

2.5. Immunofluorescence analysis

Lenses were fixed (4 °C, 12 h) in SUPER FIX (KURABO, Neyagawa, Japan) and processed using standard paraffin-section techniques. Sections were blocked (20 °C, 1 h) in 5% BSA then serially incubated with primary antibody (4 °C, 24 h) followed by secondary antibody (20 °C, 1h). Cell nuclei were stained with 4',6-diamidino-2-phenylindole (DAPI) (20 °C, 5 min) and images were captured immediately using a confocal laser fluorescence microscope (Zeiss Axio ObserverZ1). The antibodies used were anti-CHOP (Proteintech, 15204-1-AP, USA) and Alexa Fluor 488-conjugated goat anti-rabbit IgG (Thermo Fisher Scientific, R37116, USA).

2.6. TUNEL staining

Lenses were fixed in SUPER FIX and processed using standard paraffin-section techniques. Sections were subjected to TUNEL staining using In situ Apoptosis Detection Kit (TaKaRa Bio) according to the manufacturer's instructions. Briefly, eye-sections were de-waxed, digested with proteinase K (20 μg/ml, 15 min), and reacted with TdT Enzyme (37 °C, 90 min). Cell nuclei were stained with DAPI (20 °C, 5 min) and imaged with a confocal laser fluorescence microscope (Zeiss Axio Observer Z1).

2.7. Nano-flow liquid chromatography-ion trap mass spectrometry (LC-MS/MS)

Lenses were homogenized in ice-cold RIPA lysis buffer. Soluble fraction (supernatant) was separated by centrifugation (4 °C, 12,000 rpm, 15 min). The insoluble protein (pellet) was homogenized again in lysis buffer. The protein concentration in these fractions was measured using a BCA Protein Assay Kit. An aliquot equivalent to 30 μg supernatant/pellet protein of the lens lysates was separated on SDS–PAGE (12%) and stained with Coomassie Brilliant Blue. The gels of target portions (Figs. 7A and 8B) were excised and decolorized in 25 mM ammonium bicarbonate containing 50% acetonitrile solution. For reduction and alkylation of proteins, gel pierce was incubated in 10 mM dithiothreitol for 30 min on a 60 °C heating block, followed by incubation in 55 mM iodoacetamide for 45 min at room temperature in the dark. The gel pierce was dried with a Speed-Vac (TAITEC, VC-15SP, Japan) and reacted with a Pierce Trypsin Protease MS-Grade (Thermo Fisher Scientific, 90057, USA) at 37 °C for 20 h. The peptides in the gel were eluted with 50% acetonitrile solution containing 0.1% trifluoroacetic acid (TFA), dried with a Speed-Vac, and resuspended in 0.1% TFA. The samples were purified by Zip Tip C18 column (Merck Millipore, ZTC18S096, USA) according to the manufacturer's instructions, dried

A

Gene	BALB/c 4w FPKM	*Cpox*^{nct} 4w FPKM	Log2 fold change	BALB/c 12w FPKM	*Cpox*^{nct} 12w FPKM	Log2 fold change
Atf4	23.07	69.01	1.58	34.49	137.77	2.00
Chop	5.98	85.03	3.83	13.54	98.99	2.87

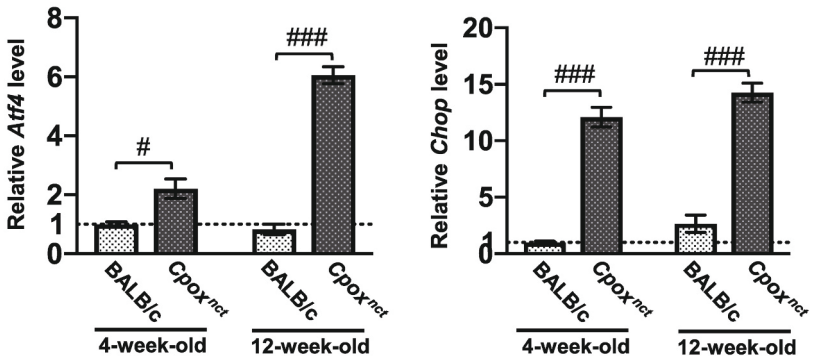

B

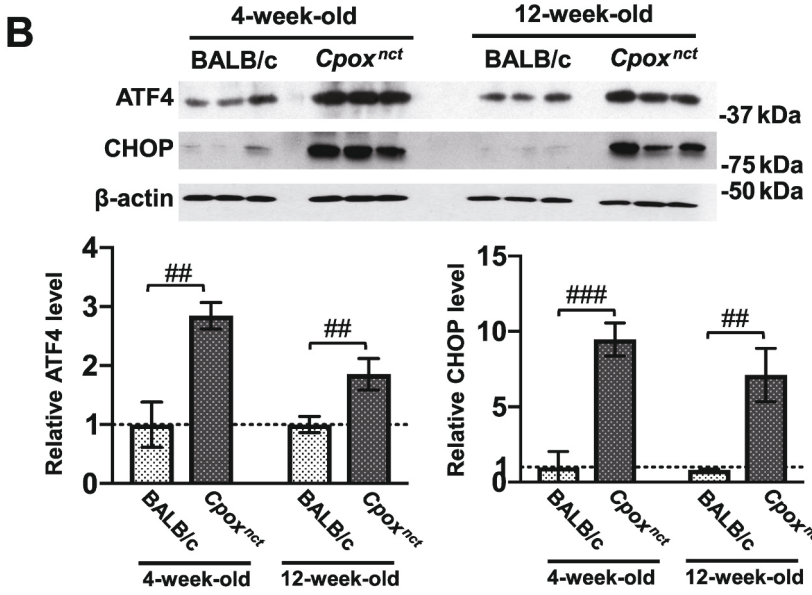

Fig. 3. ATF4 and CHOP are upregulated in the BALB.NCT-*Cpox*^{nct} lens. (**A**) RNA-seq data (top) and real-time PCR validation (bottom) of expression levels of *Atf4 and Chop* genes in the lens, normalized to β-actin (mean ± SD; n = 3). (**B**) Immuno blot images (top) and quantification (bottom) of ATF4 and CHOP in the lens, normalized to β-actin (mean ± SD; n = 3). Statistical differences between strains were evaluated using the Student's *t*-test. $^{\#}P < 0.05$, $^{\#\#}P < 0.01$, $^{\#\#\#}P < 0.001$.

again with a Speed-Vac, resuspended in 0.1% TFA, and subjected to liquid chromatography coupled online to a tandem mass spectrometer (LC-MS/MS) analysis. We used nanoflow LC-MS/MS to analyze digested peptides as described previously (Miyahara et al., 2018). Data were processed with Proteins-Lynx Global Server (PLGS) version 3.0 (Waters Corporation).

2.8. Proteasome activity assay

Lenses were homogenized in ice-cold RIPA lysis buffer without a protease inhibitor. The lens lysates were prepared by centrifugation (4 °C, 12,000 rpm, 15 min) of the homogenate. The protein concentration in the lysate was measured using a BCA Protein Assay Kit. Proteasome activity was measured using a Proteasome 20S Activity Assay Kit (Sigma-Aldrich) according to the manufacturer's instructions. Briefly, 50 μl (10 μg/μl) of the lysate was mixed with 100 μl of proteosome LLVY-R110 substrate solution of the kit and incubated at 37 °C. The change in fluorescence was monitored using a SpectraMax M5 microplate reader (Molecular Devices, San Jose, USA) with a filter set of 490 nm (excitation) and 525 nm (emission).

3. Results

3.1. Transcriptome analysis reveals a signature of increased endoplasmic reticulum stress in the BALB.NCT-Cpox^{nct} lens

To gain insights into the molecular mechanism of cataractogenesis of BALB.NCT-*Cpox*^{nct} mice, we performed transcriptome (RNA-seq) analysis to compare gene expression in the lens from BALB.NCT-*Cpox*^{nct} mice vs control BALB/c mice at 4 and 12 weeks of age. The rationale for these time points was to capture early transcriptional changes before cataractogenesis (4-week-old) and broader changes including a response to cataract formation (12-week-old). Also, a high level of coproporphyrin III is retained in the lens of BALB.NCT-*Cpox*^{nct} mice at both time points (Mori et al., 2013); ~40 nmol/g wet lens weight at 4 weeks and ~60 nmol/g wet lens weight at 12 weeks. We confirmed by visual inspection that all lenses of 12-week-old BALB.NCT-*Cpox*^{nct} mice were opaque while the lenses of other mice were transparent (Fig. 1A). We also verified that the lens weight of 4-week-old BALB.NCT-*Cpox*^{nct} was 82.1% of wild-type lens (Fig. 1B). The lens of BALB/c steadily increased in size by 12 weeks of age. In contrast, the lens of BALB.NCT-*Cpox*^{nct} showed only marginal growth in eight weeks. Consequently, the difference in the

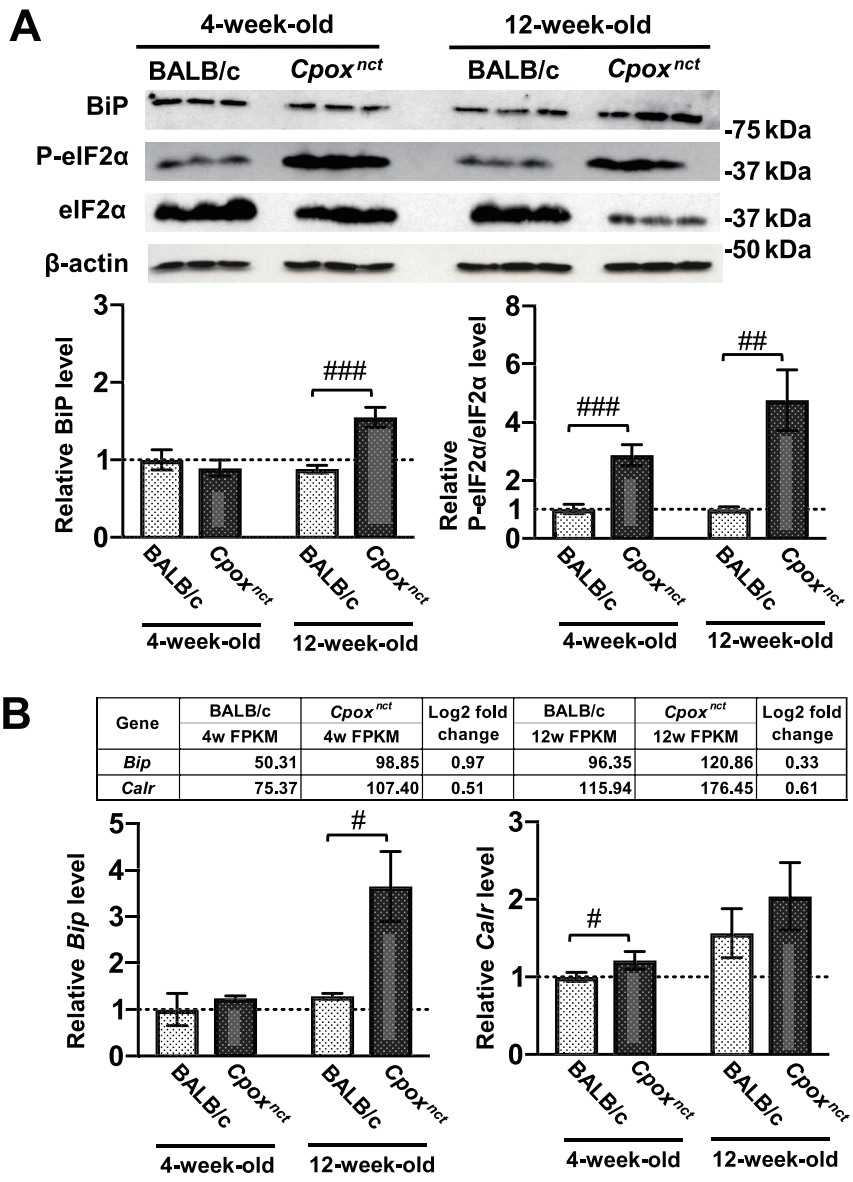

B

Gene	BALB/c 4w FPKM	*Cpox* ^{nct} 4w FPKM	Log2 fold change	BALB/c 12w FPKM	*Cpox* ^{nct} 12w FPKM	Log2 fold change
Bip	50.31	98.85	0.97	96.35	120.86	0.33
Calr	75.37	107.40	0.51	115.94	176.45	0.61

Fig. 4. PERK signaling pathway of the ER stress response is activated in the BALB.NCT-*Cpox*^{nct} lens. (**A**) Immuno blot images (top) and quantification (bottom) of BiP, P-eIF2α, and eIF2α in the lens, normalized to β-actin (mean ± SD; n = 3). (**B**) RNA-seq data (top) and real-time PCR validation (bottom) of expression levels of *Bip* and calreticulin (*Calr*) genes in the lens, normalized to β-actin (mean ± SD; n = 3). Statistical differences between strains were evaluated using the Student's *t*-test. $^{\#}P < 0.05$, $^{\#\#}P < 0.01$, $^{\#\#\#}P < 0.001$.

lens weight between BALB/c and BALB.NCT-*Cpox*^{nct} became greater at 12 weeks of age (65.8% of wild-type lens). These results were consistent with the previous report of mild microphakia in BALB.NCT-*Cpox*^{nct} (Matsuzawa et al., 1988).

As expected, a large number (1164) of differentially expressed genes (DEGs) were detected for the cataractous lens of 12-week-old (Supplementary Table 1). In contrast, only 42 DEGs were detected at 4-week-old, including 25 upregulated and 17 downregulated genes (Table 2). Of note, 28 of these 42 DEGs of the 4-week-old lens were included in the DEGs of the 12-week-old lens (Table 2; Fig. 2A and B), suggesting that the changes in the expression of these genes are central to the etiology of cataractogenesis of BALB.NCT-*Cpox*^{nct} mice. For the BALB/c lens, 118 DEGs were found between 4- and 12-week-old (Supplementary Table 2). Also, 1340 DEGs were detected between the 4- and 12-week-old BALB.NCT-*Cpox*^{nct} lenses (Supplementary Table 3). Gene ontology (GO) analysis of the 42 DEGs between the 4-week-old BALB/c and BALB.NCT-*Cpox*^{nct} lenses uncovered 51 GOs (Supplementary Table 4) including the cholesterol biosynthetic process (GO:0006695), oxidoreductase activity (GO:0016709), and endoplasmic reticulum (ER) (GO:0005783) (Fig. 2C). In the subsequent study, we focused on the GOs associated with ER.

The ER is the organelle for the proper folding and processing of proteins destined for plasma membrane or secretion. When unfolded or misfolded proteins accumulate in the ER, the cell initiates the ER stress response (or unfolded protein response; UPR) to transmit the signals from the ER to the cytoplasm and nucleus by signaling via inositol-requiring protein 1 (IRE1), activating transcription factor 6 (ATF6), and/or PKR-like endoplasmic reticulum kinase (PERK) pathways (Walter and Ron, 2011). In response to the signal, the cell induces a coordinated adaptive program to restore protein homeostasis. Activating transcription factor 4 (ATF4) and C/EBP homologous protein (CHOP) are components of the PERK pathway of the ER stress response (Walter and Ron, 2011). Namely, activated PERK increases the translation of specific mRNAs, including the *Atf4* mRNA. ATF4 turns on the expression of many downstream genes including *Chop*, to help the cell cope with the stress. Thus, upregulation of ATF4 and CHOP is a hallmark of an increase in ER stress. Intriguingly, the genes upregulated in the BALB.NCT-*Cpox*^{nct} lens included *Atf4* and *Chop* (Table 2). We validated the upregulation of *Atf4* and *Chop* transcripts by real-time RT-PCR for both 4- and 12-week-old BALB.NCT-*Cpox*^{nct} lens (Fig. 3A). In addition, we verified the increase in protein levels by immunoblotting (Fig. 3B).

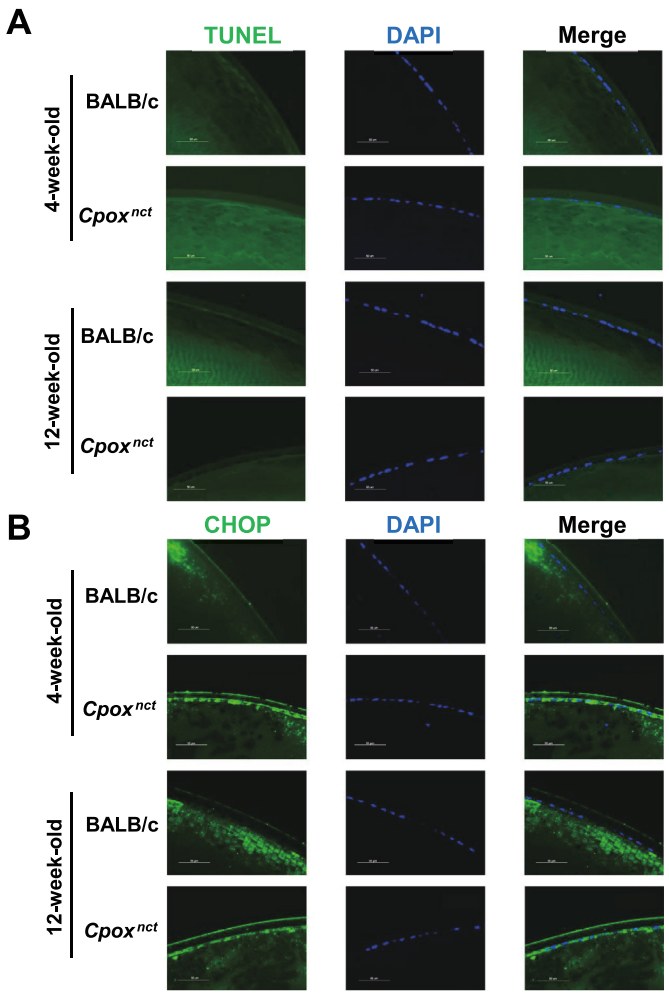

Fig. 5. Apoptosis is not exacerbated in the BALB.NCT-*Cpox*^{nct} lens. (**A**) Photomicrographs showing TUNEL staining and DAPI staining of the lens. (**B**) Immunofluorescence detection of CHOP in the lens. Scale bar, 50 μm.

3.2. *PERK signaling pathway of the ER stress response is activated in the BALB.NCT-Cpox^{nct} lens*

Because we observed upregulation of ATF4 and CHOP in BALB.NCT-*Cpox*^{nct} lens, we investigated other factors involved in the ER stress response. The activated PERK phosphorylates the translational initiation factor eIF2α (Harding et al., 1999). Phosphorylated eIF2α then represses global protein synthesis. Phosphorylated eIF2α protein level in BALB.NCT-*Cpox*^{nct} lens was increased 2.5-fold and 1.7-fold at 4- and 12 weeks the age, respectively, compared to wild-type mice (Fig. 4A). The ratio of phospho/total-eIF2α in the lens of 4-week-old BALB.NCT-*Cpox*^{nct} mice was increased threefold compared to wild-type lens. Because the total eIF2α level was decreased in 12-week-old BALB.NCT-*Cpox*^{nct} lens, the ratio of phospho/total-eIF2α was further increased to fivefold of wild-type lens (Fig. 4A). Immunoglobulin heavy chain-binding protein (BiP) (Wang et al., 2009) and calreticulin (Michalak et al., 1999) function as a molecular chaperone in the ER lumen. Both molecules are upregulated as a target of the ER stress response. In the BALB.NCT-*Cpox*^{nct} lens, the transcript and protein levels of BiP and the transcript level of calreticulin were increased at both 4 and 12 weeks of age compared to the age-matched wild-type lens (Fig. 4A and B). Collectively, these results support the deduction that unfolded/misfolded proteins accumulate in ER even before cataract development in the BALB.NCT-*Cpox*^{nct} lens that induces persistent activation of the PERK signaling pathway of the ER stress response.

3.3. *Apoptosis is not exacerbated in the BALB.NCT-Cpox^{nct} lens*

When ER stress persists and the protein load on the ER greatly exceeds its folding capacity, cellular homeostasis is disrupted, and the cell initiates the apoptosis program via upregulation and nuclear translocation of CHOP protein (Ohoka et al., 2005; Sano and Reed, 2013). Because CHOP was substantially increased in the BALB.NCT-*Cpox*^{nct} lens (Fig. 3A and B), we surmised that apoptosis is induced in the BALB/c-*Cpox*^{nct} lens. We then investigated cellular apoptosis in the BALB.NCT-*Cpox*^{nct} lens via TUNEL staining. Contrary to our expectation, no TUNEL-positive (apoptotic) cells were observed in the epithelial cells and equatorial epithelial cells, and nascent fiber cells lying outside the central degeneration zone of the BALB.NCT-*Cpox*^{nct} lens at both 4 and 12 weeks of age (Fig. 5A). Subsequently, we examined the localization of CHOP in epithelial cells of the lens via immunofluorescence. No obvious signals were observed in the epithelial cells of the wild-type lens at both 4 and 12 weeks of age (Fig. 5B). In contrast, we observed strong CHOP signals in the epithelial cells of both 4- and 12-week-old BALB.NCT-*Cpox*^{nct} lens. Intriguingly, the signals were observed in the cytoplasm rather than in the nucleus. This cytoplasmic retention of upregulated CHOP protein could account for the absence of apoptosis in the BALB.NCT-*Cpox*^{nct} lens.

3.4. *Crystallin content is reduced in the BALB.NCT-Cpox^{nct} lens*

In contrast to the transcriptional changes of a small set of genes in the lens of 4-week-old BALB.NCT-*Cpox*^{nct} mice, DEGs for the lens of 12-week-old BALB.NCT-*Cpox*^{nct} mice contained broader gene sets (Supplementary Table 1). It is worthy of notice that the transcript levels of 16 genes for crystallin isoforms were concordantly decreased to roughly 25–50% in the 12-week-old BALB.NCT-*Cpox*^{nct} lens compared with wild-type lens (Fig. 6A). At 4 weeks of age, the transcript levels of these isoforms in the BALB.NCT-*Cpox*^{nct} lens were only slightly decreased (Fig. 6A). We validated the decrease in the transcript levels of αA-crystallin (*Cryaa*) and αB-crystallin (*Cryab*) in the 12-week-old BALB.NCT-*Cpox*^{nct} lens by real-time RT-PCR (Fig. 6A). Also, consistent with the RNA-seq data, protein levels of αB-crystallin (CRYAB) and βB1-crystallin (CRYBB1) in the 12-week-old BALB.NCT-*Cpox*^{nct} lens were significantly decreased (Fig. 6B).

3.5. *Crystallin and keratin are aggregated in the BALB.NCT-Cpox^{nct} lens*

In addition to the change in amount, we examined the status of crystallins and other proteins further. For this objective, we separated the lens lysate of 4- and 12-week-old mice into soluble and insoluble fractions by centrifugation. Lenses of 12-week-old BALB.NCT-*Cpox*^{nct} mice were opaque while the lenses of other mice were transparent. Soluble proteins were further separated by SDS-PAGE followed by Coomassie Brilliant Blue staining. Intriguingly, a dense band at the top of the gel indicative of stacking protein aggregates was observed for the BALB.NCT-*Cpox*^{nct} lens of both 4 and 12 weeks of age (Fig. 7A). This stacking band was not apparent for the wild-type lens. We then excised the high molecular mass region (>250 kDa) from the gel, extracted the materials from the gel piece, and identified the proteins by LC mass spectrometry. Consistent with the absence of a stacking band, no protein was detected from the lens of 4-week-old wild-type mice (Fig. 7B). Similarly, only type II cytoskeletal keratin was detected in the 12-week-old wild-type lens. In contrast, the lens of both 4- and 12-week-old BALB.NCT-*Cpox*^{nct} mice contained various keratin and crystallin isoforms (Fig. 7B). Damaged or unneeded proteins in the cytoplasm and nucleus are degraded by the proteasome. In agreement with the accumulation of protein aggregates, the proteasome activity was approximately 3–4 folds in the 12-week-old opaque BALB.NCT-*Cpox*^{nct} lens and even in the transparent lens of 4-week-old mice compared to age-matched wild-type lens (Fig. 7C).

A

Gene	BALB/c 4w FPKM	*Cpox*^{nct} 4w FPKM	Log2 fold change	BALB/c 12w FPKM	*Cpox*^{nct} 12w FPKM	Log2 fold change
Cryaa	155191	164087	0.08	133001	88644	-0.59
Cryab	19307	17242	-0.16	13031	9398	-0.47
Cryba1	76148	64877	-0.23	39756	30162	-0.40
Cryba2	15225	13817	-0.14	18892	10713	-0.82
Cryba4	28120	25398	-0.15	25843	11550	-1.16
Crybb1	28290	26862	-0.08	16428	13826	-0.25
Crybb2	164583	171778	0.06	229733	149755	-0.62
Crybb3	33082	31399	-0.08	15193	11735	-0.37
Cryga	274	273	0.00	6	3	-1.00
Crygb	50538	44509	-0.18	24590	10038	-1.29
Crygc	76635	4442	-0.77	28276	12093	-1.23
Crygd	109299	85006	-0.36	33262	22446	-0.57
Cryge	47928	38625	-0.31	808	347	-1.22
Crygf	18290	14535	-0.33	918	766	-0.26
Crygn	1191	766	-0.64	186	158	-0.24
Crygs	58784	42289	-0.48	4415	20272	-1.12

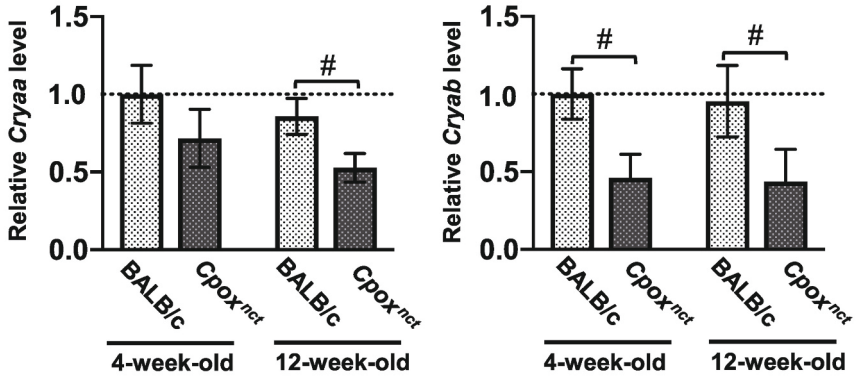

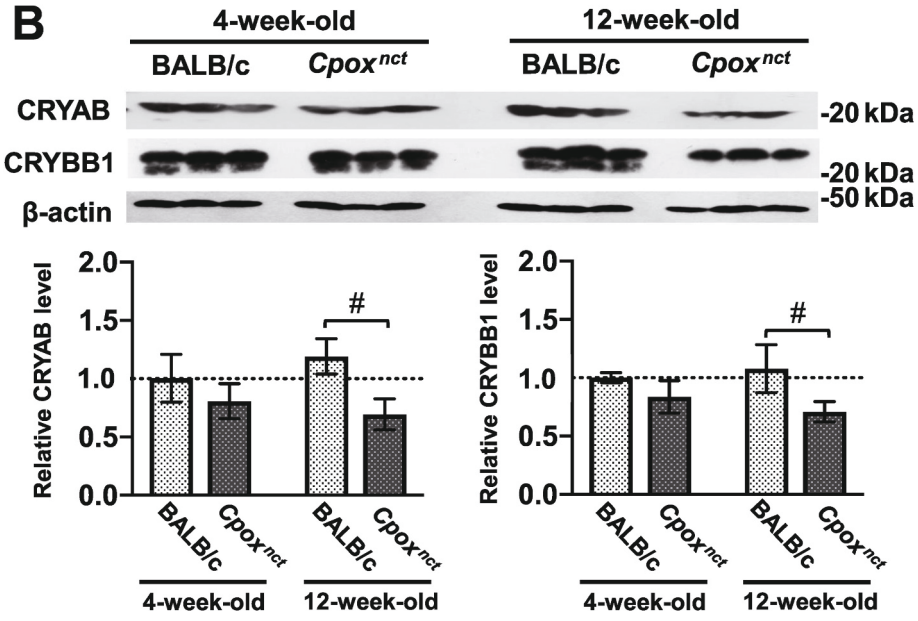

Fig. 6. Crystallin content is reduced in the BALB.NCT-*Cpox*^{nct} lens. (**A**) RNA-seq data for crystallin genes (top) and real-time PCR validation of *Cryaa* and *Cryab* genes (bottom) in the lens, normalized to β-actin (mean ± SD; n = 3). (**B**) Immuno blot images (top) and quantification (bottom) of CRYAB and CRYBB1 in the lens, normalized to β-actin (mean ± SD; n = 3). Statistical differences between strains were evaluated using the Student's *t*-test. $^{\#}P < 0.05$.

3.6. *Insoluble crystallins and keratins are accumulated in the cataractous BALB.NCT-Cpox*^{nct} *lens*

We also investigated insoluble proteins in the lens. Only a small amount of insoluble proteins was observed in the transparent lenses of 4-week-old BALB/c and BALB.NCT-*Cpox*^{nct} mice (Fig. 8A). In contrast, a large amount of insoluble protein was obtained from the cataractous lens of 12-week-old BALB.NCT-*Cpox*^{nct} mice. To analyze the composition of the insoluble proteins, we separated the proteins by SDS-PAGE. We then excised the high molecular mass regions of the gel, extracted the materials from the gel piece, and identified the proteins by LC mass spectrometry (Fig. 8B). Insoluble proteins from the 12-week-old wild-type lens contained keratin isoforms (Fig. 8C). Notably, in addition to keratins, various crystallin isoforms including CRYAA, CRYGA, CRYGB, CRYBA, CRYBB2, and CRYBB1 were included in the insoluble protein fraction of cataractous lens of 12-week-old BALB.NCT-*Cpox*^{nct} mice.

4. Discussion

In this study, we clarified the molecular events and changes in

A

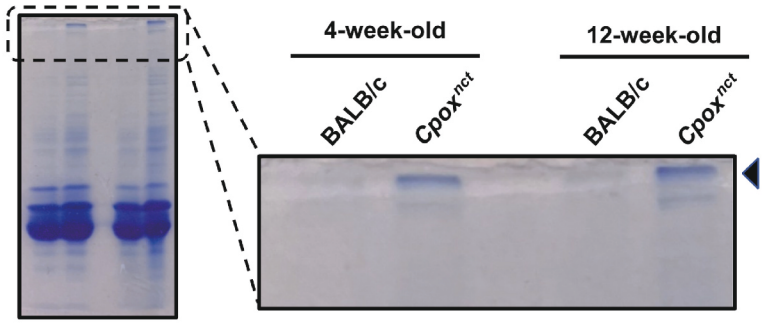

B

Sample	Protein	Sample	Protein
BALB/c-4w supernatant	none	*Cpox*^{nct}-4w supernatant	Keratin type I cytoskeletal 9
			Keratin type I cytoskeletal 10
			Keratin type I cytoskeletal 14
			Keratin type I cytoskeletal 17
			Keratin type II cytoskeletal 1
			Keratin type II cytoskeletal 2
			Keratin type II cytoskeletal 5
			Keratin type II cytoskeletal 6A
			Keratin type II cytoskeletal 6D
			Keratin intermediate filament 16b
			Beta B1 crystallin
			Beta A3 A1 crystallin
			MKIAA0845
Sample	Protein	Sample	Protein
BALB/c-12w supernatant	Keratin type II cytoskeletal 1	*Cpox*^{nct}-12w supernatant	Keratin type I cytoskeletal 9
	Uncharacterized protein		Keratin type I cytoskeletal 10
			Keratin type I cytoskeletal 14
			Keratin type I cytoskeletal VIB
			Keratin type II cytoskeletal 1
			Keratin type II cytoskeletal 2
			Keratin type II cytoskeletal 71
			Keratin type II cytoskeletal 73
			Keratin type II cytoskeletal 74
			Keratin 77
			Beta B1 crystallin
			Beta A3 A1 crystallin

C

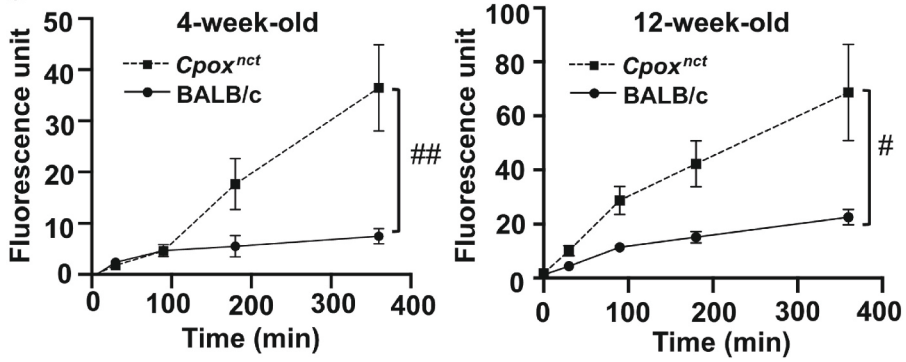

Fig. 7. Crystallin and keratin are aggregated in the BALB.NCT-*Cpox*^{nct} lens. (**A**) An image of Coomassie Brilliant Blue-stained SDS-PAGE gel for separation of soluble protein aggregates in the BALB.NCT-*Cpox*^{nct} lens. The arrowhead indicates the protein aggregates stacking at the top of the gel that were subjected to the LC mass spectrometry analysis. (**B**) A list of the identified proteins in aggregates. (**C**) Proteasome activity in the lens of BALB/c and BALB.NCT-*Cpox*^{nct} (mean ± SD; n = 3). Statistical differences between strains were evaluated using the Student's *t*-test. $^{\#}P < 0.05$, $^{\#\#}P < 0.01$.

transcripts and proteins of the BALB.NCT-*Cpox*^{nct} lens. Based on the obtained results, we infer the sequence of molecular events that lead to cataracts in BALB.NCT-*Cpox*^{nct} (Fig. 9): chronic accumulation of coproporphyrin induces aggregation of proteins including crystallins. Aggregated proteins increase ER stress that, in turn, leads to repression of global translation of proteins including molecular chaperone crystallins. The decline in the crystallin aggravates aggregation and insolubilization of proteins. This vicious cycle would eventually lead to cataracts in BALB.NCT-*Cpox*^{nct}.

We found that the aggregation of keratins and crystallins was formed in the BALB.NCT-*Cpox*^{nct} lens prior to the manifestation of cataracts (4 weeks of age). We surmise that an incipient event in the BALB.NCT-*Cpox*^{nct} lens is this aggregation of proteins presumably caused by accumulated coproporphyrin. The data obtained in this study do not conclusively prove the causal relationship of accumulated coproporphyrin to protein aggregation in the BALB.NCT-*Cpox*^{nct} lens. Intriguingly, several papers demonstrated that coproporphyrin binds proteins possibly through the deprotonation of the carboxylate moiety of the propionic acid side chain, and leads, in the presence of oxygen, to protein oxidation and aggregation in the liver of inducible mouse models of porphyria (Singla et al., 2013; Maitra et al., 2015, 2019b; Maitra et al., 2019a). Thus, it is likely that accumulated coproporphyrin aggregates proteins in the BALB.NCT-*Cpox*^{nct} lens by this mechanism. Also, previous studies with cultured cells and a zebrafish model revealed that accumulated coproporphyrin aggregates ER-resident proteins (e.g., protein disulfide isomerase; PDI) and induces ER stress (Maitra et al., 2015; Elenbaas et al., 2016).

Consistent with these reports, we observed increased ER stress in the BALB.NCT-*Cpox*^{nct} lens that was exemplified by persistent activation of the PERK signaling pathway of the ER stress response. Involvement of

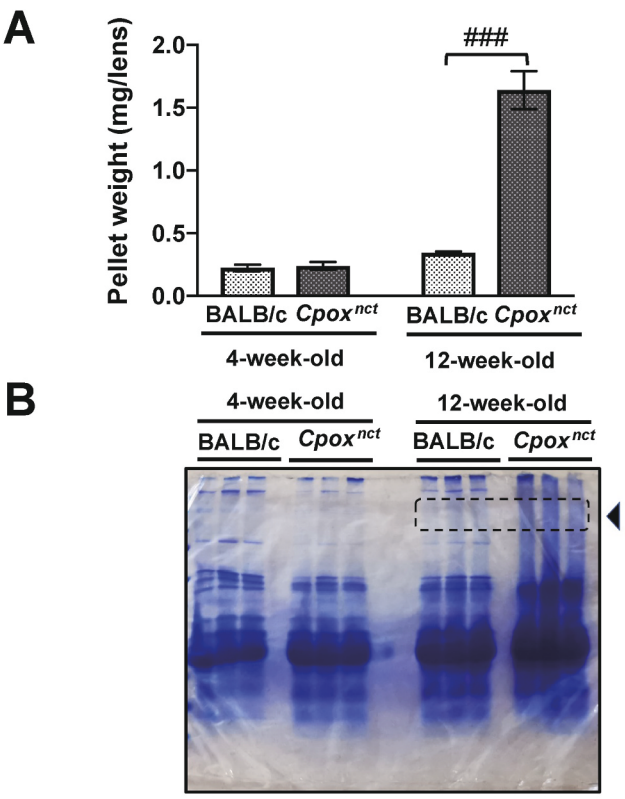

Fig. 8. Insoluble crystallins and keratins are accumulated in the cataractous BALB.NCT-*Cpox*^{nct} lens. (**A**) Comparison of the amount of insoluble protein pellet collected from the lens. (**B**) An image of Coomassie Brilliant Blue-stained SDS-PAGE gel for separation of insoluble proteins in the lens. The arrowhead indicates the excised gel area for the LC mass spectrometry analysis. (**C**) A list of the identified proteins in the excised gel. Statistical differences between strains were evaluated using the Student's *t*-test. $^{###}P < 0.001$

C

Sample	Protein	Sample	Protein
BALB/c-12w pellet	Keratin type I cytoskeletal 9	*Cpox* ^{nct}-12w pellet	Keratin type I cytoskeletal 9
	Keratin type I cytoskeletal 10		Keratin type I cytoskeletal 10
	Keratin type II cytoskeletal 1		Keratin type II cytoskeletal 1
	Keratin type II cytoskeletal 2		Keratin type II cytoskeletal 2
			Alpha A crystallin (CRYAA)
			Gamma A crystallin (CRYGA)
			Gamma B crystallin (CRYBGB)
			Beta A3 A1 crystallin (CRYBA)
			Beta B2 crystallin (CRYBB2)
			Beta B1 crystallin (CRYBB1)

ER stress in cataract formation has been demonstrated in other cataract mouse models (Ma et al., 2016; Berthoud et al., 2016; Zhou et al., 2016; Huang et al., 2021), human lens epithelial cell culture model (Zhou et al., 2020), and cataracts in humans (Yang et al., 2015). Our data reinforce the importance of ER stress in the etiology of cataracts (Ikesugi et al., 2006; Periyasamy and Shinohara, 2017). An outcome of activation of the PERK signaling pathway under ER stress is repression of global protein translation (Pavitt, 2005; Jennings and Pavitt, 2014; Perry et al., 2018). A previous study of the NCT lens revealed a drastic reduction in the translation of persistent crystallin mRNA in fiber cells and a milder reduction in the translation of crystallins in epithelial cells (Shinohara and Piatigorsky, 1980). Consistent with this report, we observed that crystallin content was reduced in the BALB.NCT-*Cpox*^{nct} lens. Although we did not demonstrate repression of global protein translation in the BALB.NCT-*Cpox*^{nct} lens, persistent translational repression due to aggravated ER stress could be responsible for these features and even for retarded growth of the lens of BALB.NCT-*Cpox*^{nct} (Fig. 1; Matsuzawa et al., 1988) and NCT (Fukui et al., 1976). In addition, previous studies demonstrated that ER stress activates the expression of genes involved in cholesterol biosynthesis (Werstuck et al., 2001; Lee and Ye, 2004; Colgan et al., 2007; Kim et al., 2018). In agreement with these reports, the RNA-seq data indicated that the cholesterol biosynthetic process is upregulated in the BALB.NCT-*Cpox*^{nct} lens (Table 2 and Supplementary Table 4). Although we cannot deny the possibility that activation of the cholesterol biosynthetic process is causally linked to cataractogenesis in BALB.NCT-*Cpox*^{nct}, it is more likely that the upregulation of the cholesterol biosynthesis observed in the BALB.NCT-*Cpox*^{nct} lens is a subsidiary response to an increase in ER stress.

However, there remains an issue to be solved to establish an etiological link of increased ER stress to cataracts of BALB.NCT-*Cpox*^{nct} mice. Specifically, misfolded/unfolded protein that causes ER stress in the BALB.NCT-*Cpox*^{nct} lens is unknown. CPOX mutated in BALB.NCT-*Cpox*^{nct} mice is a mitochondrial protein and does not go through ER during production. Therefore, it is unlikely that mutant CPOX with the p.R380L amino acid substitution is the direct cause of ER stress. In previous studies with cultured cells and a zebrafish model, it was demonstrated that the ER-resident PDI was aggregated by coproporphyrin III (Maitra et al., 2015; Elenbaas et al., 2016). However, LC mass analysis of aggregated proteins in BALB.NCT-*Cpox*^{nct} lens failed to detect ER-related proteins including PDI. RNA-seq data in this study indicated that the level of transcripts for PDI was extremely low in the lens. Furthermore, PDI was undetectable in the immunoblot of the mouse lens (data not shown). These results suggested that the content of PDI in the lens was below measurable limits. In contrast, aggregates of ER-related proteins were observed in the liver of BALB.NCT-*Cpox*^{nct} mice containing excessive coproporphyrin (data not shown), suggesting the

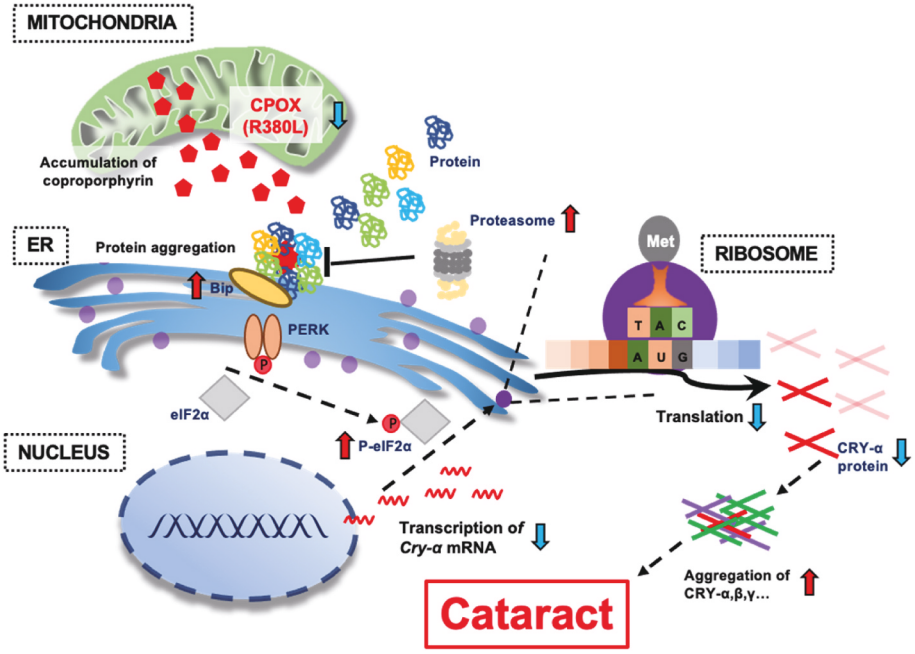

Fig. 9. Hypothetical mechanism of cataractogenesis in BALB.NCT-*Cpox*^{nct} mice. The diagram summarizes the molecular events observed in the BALB.NCT-*Cpox*^{nct} lens. Coproporphyrin accumulation induces ER stress, leading to activation of the PERK-mediated pathway in the BALB.NCT-*Cpox*^{nct} lens. Phosphorylated eIF2α inhibits the translation of CRY-a and exacerbates aggregation and insolublilization of crystallins. The sequence of molecular events eventually leads to cataracts and microphakia in BALB.NCT-*Cpox*^{nct} mice.

possibility that ER of the BALB.NCT-*Cpox*^{nct} lens contained a trace amount of protein aggregates as well.

Intriguingly, RNA-seq analysis indicated that transcripts of all crystallin are simultaneously reduced. The mechanism for this simultaneous reduction of crystallin transcripts is currently unclear. It may occur as a part of the negative feedback regulation of crystallin production under ER stress. The importance of crystallins in the lens is twofold. First, crystallins are the major constitutive proteins of the lens fiber cells. In this context, crystallins are essential to growth and maintenance of the lens. Also, they function to increase the refractive index while not obstructing light. Second, α-crystallin which is constituted by two polypeptides of αA and αB possesses chaperone-like properties (Bloemendal et al., 2004). In this context, α-crystallin works also to maintain lens transparency by preventing the precipitation of denatured proteins. Mature lens fiber cells are devoid of machinery for protein synthesis and degradation. Hence, these cells cannot eliminate and replenish denatured proteins. Thus, the reduction in crystallins in the BALB.NCT-*Cpox*^{nct} lens should promote the formation of cataracts.

Finally, we address the relevance of our findings in BALB.NCT-*Cpox*^{nct} to humans. CPOX mutations in humans give rise to hereditary coproporphyria (Schmitt et al., 2005). To the best of our knowledge, there has been no report of complications of cataracts in these patients. The absence of cataracts in coproporphyria patients could be due to the incomplete penetrance of the disorder (Hasanoglu et al., 2011). Thus, different from the chronic spontaneous accumulation of coproporphyrin in the BALB.NCT-*Cpox*^{nct} lens, a surge of coproporphyrin content in the blood and organs in these patients is generally intermittent. Symptoms are often provoked by exogenous causes such as drugs, fasting, menstrual cycle, or infectious diseases. Nevertheless, we cannot preclude the possibility that frequent intermittent surge of coproporphyrin in the lens increases risks of cataracts later in their life. A careful ophthalmic follow-up would then be beneficial for these patients.

Funding

This work was supported in part by Grants-in-Aid for Scientific Research (C) from the Ministry of Education, Culture, Sports, Science and Technology, Japan [grant number 19K06455].

Conflict of interest

The authors have no conflict of interest.

Declaration of competing interest

None.

Acknowledgments

We thank RIKEN BRC (Tsukuba, Japan) and the National Bio-Resource Project of MEXT/AMED (Tokyo, Japan) for providing us with a BALB.NCT-*Cpox*^{nct} strain.

Appendix A. Supplementary data

Supplementary data to this article can be found online at https://doi.org/10.1016/j.exer.2021.108905.

References

Anders, S., Pyl, P.T., Huber, W., 2015. HTSeq–a Python framework to work with high-throughput sequencing data. Bioinformatics 31, 166–169. https://doi.org/10.1093/bioinformatics/btu638.

Andley, U.P., Tycksen, E., McGlasson-Naumann, B.N., Hamilton, P.D., 2018. Probing the changes in gene expression due to alpha-crystallin mutations in mouse models of hereditary human cataract. PLoS One 13, e0190817. https://doi.org/10.1371/journal.pone.0190817.

Benjamini, Y., Hochberg, Y., 1995. Controlling the false discovery rate: a practical and powerful approach to multiple testing. J. Roy. Statist. Soc. Ser. B57, 289–300, 1995.

Bennett, T.M., Zhou, Y., Shiels, A., 2016. Lens transcriptome profile during cataract development in Mip-null mice. Biochem. Biophys. Res. Commun. 478, 988–993. https://doi.org/10.1016/j.bbrc.2016.08.068.

Berthoud, V.M., Minogue, P.J., Lambert, P.A., Snabb, J.I., Beyer, E.C., 2016. The cataract-linked mutant connexin50D47A causes endoplasmic reticulum stress in mouse lenses. J. Biol. Chem. 291, 17569–17578. https://doi.org/10.1074/jbc.M115.707950.

Bloemendal, H., de Jong, W., Jaenicke, R., Lubsen, N.H., Slingsby, C., Tardieu, A., 2004. Ageing and vision: structure, stability and function of lens crystallins. Prog. Biophys. Mol. Biol. 86, 407–485. https://doi.org/10.1016/j.pbiomolbio.2003.11.012.

Colgan, S.M., Tang, D., Werstuck, G.H., Austin, R.C., 2007. Endoplasmic reticulum stress causes the activation of sterol regulatory element binding protein-2. Int. J. Biochem. Cell Biol. 39, 1843–1851. https://doi.org/10.1016/j.biocel.2007.05.002.

Elenbaas, J.S., Maitra, D., Liu, Y., Lentz, S.I., Nelson, B., Hoenerhoff, M.J., Shavit, J.A., Omary, M.B., 2016. A precursor-inducible zebrafish model of acute protoporphyria

with hepatic protein aggregation and multiorganelle stress. Faseb. J. 30, 1798–1810. https://doi.org/10.1096/fj.201500111R.
Fukui, H.N., Obazawa, H., Kinoshita, J.H., 1976. Lens growth in the Nakano mouse. Invest. Ophthalmol. 15, 422–425.
Harding, H.P., Zhang, Y., Ron, D., 1999. Protein translation and folding are coupled by an endoplasmic-reticulum-resident kinase. Nature 397, 271–274. https://doi.org/10.1038/16729.
Hasanoglu, A., Balwani, M., Kasapkara, C.S., Ezgu, F.S., Okur, I., Tumer, L., Cakmak, A., Nazarenko, I., Yu, C., Clavero, S., Bishop, D.F., Desnick, R.J., 2011. Harderoporphyria due to homozygosity for coproporphyrinogen oxidase missense mutation H327R. J. Inherit. Metab. Dis. 34, 225–231. https://doi.org/10.1007/s10545-010-9237-9.
Hegde, S.M., Srivastava, K., Tiwary, E., Srivastava, O.P., 2014. Molecular mechanism of formation of cortical opacity in CRYAAN101D transgenic mice. Invest. Ophthalmol. Vis. Sci. 55, 6398–6408. https://doi.org/10.1167/iovs.14-14623.
Huang, Y., Ye, Z., Yin, Y., Ma, T., Zhang, Q., Shang, K., Chen, W., Li, Z., 2021. Cataract formation in transgenic HO-1 G143H mutant mice: involvement of oxidative stress and endoplasmic reticulum stress. Biochem. Biophys. Res. Commun. 537, 43–49. https://doi.org/10.1016/j.bbrc.2020.12.071.
Ikesugi, K., Yamamoto, R., Mulhern, M.L., Shinohara, T., 2006. Role of the unfolded protein response (UPR) in cataract formation. Exp. Eye Res. 83, 508–516.
Ishida, H., Shibata, T., Nakamura, Y., Ishigaki, Y., Singh, D.P., Sasaki, H., Kubo, E., 2020. Identification of differential gene expression pattern in lens epithelial cells derived from cataractous and noncataractous lenses of Shumiya cataract rat. BioMed Res. Int. 2020, 7319590. https://doi.org/10.1016/j.exer.2006.01.033.
Jennings, M.D., Pavitt, G.D., 2014. A new function and complexity for protein translation initiation factor eIF2B. Cell Cycle 13, 2660–2665. https://doi.org/10.4161/15384101.2014.948797.
Jia, Z.K., Fu, C.X., Wang, A.L., Yao, K., Chen, X.J., 2021. Cataract-causing allele in CRYAA (Y118D) proceeds through endoplasmic reticulum stress in mouse model. Zool. Res. 42, 300–309. https://doi.org/10.24272/j.issn.2095-8137.2020.354.
Kim, D., Pertea, G., Trapnell, C., Pimentel, H., Kelley, R., Salzberg, S.L., 2013. TopHat2: accurate alignment of transcriptomes in the presence of insertions, deletions and gene fusions. Genome Biol. 14, R36. https://doi.org/10.1186/gb-2013-14-4-r36.
Kim, J.Y., Garcia-Carbonell, R., Yamachika, S., Zhao, P., Dhar, D., Loomba, R., Kaufman, R.J., Saltiel, A.R., Karin, M., 2018. ER stress drives lipogenesis and steatohepatitis via caspase-2 activation of S1P. Cell 175, 133–145. https://doi.org/10.1016/j.cell.2018.08.020 e15.
Koyama-Ito, H., Wada, E., 1992. Elemental distribution in frozen-hydrated mouse lenses with hereditary cataract. Lens Eye Toxic. Res. 9, 55–65.
Lee, J.N., Ye, J., 2004. Proteolytic activation of sterol regulatory element-binding protein induced by cellular stress through depletion of Insig-1. J. Biol. Chem. 279, 45257–45265. https://doi.org/10.1074/jbc.M408235200.
Ma, Z., Yao, W., Chan, C.C., Kannabiran, C., Wawrousek, E., Hejtmancik, J.F., 2016. Human betaA3/A1-crystallin splicing mutation causes cataracts by activating the unfolded protein response and inducing apoptosis in differentiating lens fiber cells. Biochim. Biophys. Acta 1862, 1214–1227. https://doi.org/10.1016/j.bbadis.2016.02.003.
Maitra, D., Bragazzi Cunha, J., Elenbaas, J.S., Bonkovsky, H.L., Shavit, J.A., Omary, M. B., 2019a. Porphyrin-induced protein oxidation and aggregation as a mechanism of porphyria-associated cell injury. Cell. Mol. Gastroenterol. Hepatol. 8, 535–548. https://doi.org/10.1016/j.jcmgh.2019.06.006.
Maitra, D., Carter, E.L., Richardson, R., Rittie, L., Basrur, V., Zhang, H., Nesvizhskii, A., Osawa, Y., Wolf, M.W., Ragsdale, S.W., Lehnert, N., Hermann, H., Omary, M.B., 2019b. Oxygen and conformation dependent protein oxidation and aggregation by porphyrins in hepatocytes and light-exposed cells. Cell. Mol. Gastroenterol. Hepatol. 8, 659–682. https://doi.org/10.1016/j.jcmgh.2019.05.010.
Maitra, D., Elenbaas, J.S., Whitesall, S.E., Basrur, V., D'Alecy, L.G., Omary, M.B., 2015. Ambient light promotes selective subcellular proteotoxicity after endogenous and exogenous porphyrinogenic stress. J. Biol. Chem. 290, 23711–23724. https://doi.org/10.1074/jbc.M114.636001.
Matsuzawa, A., Wada, E., 1988. Retarded and distinct progress of lens opacification in congenic hereditary cataract mice, Balb/c-nct/nct. Exp. Eye Res. 47, 705–711. https://doi.org/10.1016/0014-4835(88)90038-3.
Michalak, M., Corbett, E.F., Mesaeli, N., Nakamura, K., Opas, M., 1999. Calreticulin: one protein, one gene, many functions. Biochem. J. 344, 281–292.
Miyahara, H., Sawashita, J., Ishikawa, E., Yang, M., Ding, X., Liu, Y., Hachiya, N., Kametani, F., Yazaki, M., Mori, M., Higuchi, K., 2018. Comprehensive proteomic profiles of mouse AApoAII amyloid fibrils provide insights into the involvement of lipoproteins in the pathology of amyloidosis. J. Proteonomics 172, 111–121. https://doi.org/10.1016/j.jprot.2017.10.003.
Mori, M., Gotoh, S., Taketani, S., Hiai, H., Higuchi, K., 2013. Hereditary cataract of the Nakano mouse: involvement of a hypomorphic mutation in the coproporphyrinogen oxidase gene. Exp. Eye Res. 112, 45–50. https://doi.org/10.1016/j.exer.2013.04.005.
Nakano, K., Yamamoto, S., Kutsukake, G., Ogawa, H., Nakajima, A., Takano, E., 1960. Hereditary cataract in mice. Jpn. J. Clin. Ophthalmol. 14, 1772–1776.
Ohoka, N., Yoshii, S., Hattori, T., Onozaki, K., Hayashi, H., 2005. TRB3, a novel ER stress-inducible gene, is induced via ATF4-CHOP pathway and is involved in cell death. EMBO J. 24, 1243–1255. https://doi.org/10.1038/sj.emboj.7600596.
Pavitt, G.D., 2005. eIF2B, a mediator of general and gene-specific translational control. Biochem. Soc. Trans. 33 https://doi.org/10.1042/BST20051487, 1498-1492.
Periyasamy, P., Shinohara, T., 2017. Age-related cataracts: role of unfolded protein response, Ca^{2+} mobilization, epigenetic DNA modifications, and loss of Nrf2/Keap1 dependent cytoprotection. Prog. Retin. Eye Res. 60, 1–19. https://doi.org/10.1016/j.preteyeres.2017.08.003.
Perry, B.D., Rahnert, J.A., Xie, Y., Zheng, B., Woodworth-Hobbs, M.E., Price, S.R., 2018. Palmitate-induced ER stress and inhibition of protein synthesis in cultured myotubes does not require Toll-like receptor 4. PLoS One 13, e0191313. https://doi.org/10.1371/journal.pone.0191313.
Sano, R., Reed, J.C., 2013. ER stress-induced cell death mechanisms. Biochim. Biophys. Acta 1833, 3460–3470. https://doi.org/10.1016/j.bbamcr.2013.06.028.
Schmitt, C., Gouya, L., Malonova, E., Lamoril, J., Camadro, J.-M., Flamme, M., Rose, C., Lyoumi, S., Da Silva, V., Boileau, C., Grandchamp, B., Beaumont, C., Deybach, J.-C., Puy, H., 2005. Mutations in human CPO gene predict clinical expression of either hepatic hereditary coproporphyria or erythropoietic harderoporphyria. Hum. Mol. Genet. 14, 3089–3098. https://doi.org/10.1093/hmg/ddi342.
Shinohara, T., Piatigorsky, J., 1980. Persistence of crystallin messenger RNA's with reduced translation in hereditary cataracts in mice. Science 210, 914–916. https://doi.org/10.1126/science.7434006.
Singla, A., Griggs, N.W., Kwan, R., Snider, N.T., Maitra, D., Ernst, S.A., Hermann, H., Omary, M.B., 2013. Lamin aggregation is an early sensor of porphyria-induced liver injury. J. Cell Sci. 126, 3105–3112. https://doi.org/10.1242/jcs.123026.
Takehana, M., 1990. Hereditary cataract of the Nakano mouse. Exp. Eye Res. 50, 671–676. https://doi.org/10.1016/0014-4835(90)90112-8.
Trapnell, C., Williams, B.A., Pertea, G., Mortazavi, A., Kwan, G., van Baren, M.J., Salzberg, S.L., Wold, B.J., Pachter, L., 2010. Transcript assembly and quantification by RNA-seq reveals unannotated transcripts and isoform switching during cell differentiation. Nat. Biotechnol. 28, 511–515. https://doi.org/10.1038/nbt.1621.
Wada, E., Koyama-Ito, H., Matsuzawa, A., 1991. Biochemical evidence for conversion to milder form of hereditary mouse cataract by different genetic background. Exp. Eye Res. 52, 501–506. https://doi.org/10.1016/0014-4835(91)90049-k.
Walter, P., Ron, D., 2011. The unfolded protein response: from stress pathway to homeostatic regulation. Science 334. https://doi.org/10.1126/science.1209038, 1091-1086.
Wang, L., Feng, Z., Wang, X., Wang, X., Zhang, X., 2010. DEGseq: an R package for identifying differentially expressed genes from RNA-seq data. Bioinformatics 26, 136–138. https://doi.org/10.1093/bioinformatics/btp612.
Wang, M., Wey, S., Zhang, Y., Ye, R., Lee, A.S., 2009. Role of the unfolded protein response regulator GRP78/BiP in development, cancer, and neurological disorders. Antioxidants Redox Signal. 11, 2307–2316. https://doi.org/10.1089/ars.2009.2485.
Wang, Z., Su, D., Liu, S., Zheng, G., Zhang, G., Cui, T., Ma, X., Sun, Z., Hu, S., 2021. RNA sequencing and bioinformatics analysis of human lens epithelial cells in age-related cataract. BMC Ophthalmol. 21, 152. https://doi.org/10.1186/s12886-021-01915-5.
Werstuck, G.H., Lentz, S.R., Dayal, S., Hossain, G.S., Sood, S.K., Shi, Y.Y., Zhou, J., Maeda, N., Krisans, S.K., Malinow, M.R., Austin, R.C., 2001. Homocysteine-induced endoplasmic reticulum stress causes dysregulation of the cholesterol and triglyceride biosynthetic pathways. J. Clin. Invest. 107, 1263–1273. https://doi.org/10.1172/JCI11596.
Yamamoto, Y., Iwata, S., 1973. Implantation of crystalline lens in mice: as one of the approaches for cataract study. Acta Soc. Ophthalmol. Jpn. 77, 888–896.
Yang, J., Zhou, S., Gu, J., Wang, Y., Guo, M., Liu, Y., 2015. Differences in unfolded protein response pathway activation in the lenses of three types of cataracts. PLoS One 10, e0130705. https://doi.org/10.1371/journal.pone.0130705.
Young, M.D., Wakefield, M.J., Smyth, G.K., Oshlack, A., 2010. Gene ontology analysis for RNA-seq: accounting for selection bias. Genome Biol. 11, R14. https://doi.org/10.1186/gb-2010-11-2-r14.
Zhou, S., Yang, J., Wang, M., Zheng, D., Liu, Y., 2020. Endoplasmic reticulum stress regulates epithelial-mesenchymal transition in human lens epithelial cells. Mol. Med. Rep. 21, 173–180. https://doi.org/10.3892/mmr.2019.10814.
Zhou, Y., Bennett, T.M., Shiels, A., 2016. Lens ER-stress response during cataract development in Mip-mutant mice. Biochim. Biophys. Acta 1862, 1433–1442. https://doi.org/10.1016/j.bbadis.2016.05.003.